LoRa System for Search and Rescue: Path Loss Models and Procedures in Mountain Scenarios

G. M. Bianco, R. Giuliano, G. Marrocco, F. Mazzenga, A. Mejia-Aguilar

***Abstract*—Typical mountain Search and Rescue (SaR) operations require the localization of the persons involved in accidents in harsh environments. ARVA and RECCO® are the current standards for the localization in snowy environments although their radio range is limited to some tens of meters. In this paper, we prove by experimental results that the Long Range (LoRa) Low-Power Wide-Area Network (LPWAN) technology is very promising for SaR applications due to its extended radio range. A LoRa-based system for SaR operations is presented and analyzed. The localization of the persons is obtained through an algorithm based on path loss measurements. Radio path loss models of body-worn LoRa devices in harsh mountain environments are derived by measurements. We observed that, although the communication range of LoRa decreases from kilometres to hundreds of meters in the tested environments, at least 50% of the transmitted packets can be received at distances about five times greater than those achievable with golden standard technologies such as ARVA. The performances of the considered localization algorithm are analyzed on the basis of the collected data. The achievable accuracy is in the order of meters around the true position for a relatively large number of available path loss measurements. Lastly, we propose and detail a LoRa-based system for SaR operations.**

***Index Terms*—Body Area IoT, LoRa, LPWAN, path loss, range, Search and Rescue**

I. Introduction

Winter mountain sports and activities are very popular all over the world. In the case of an accident, for successful Search and Rescue (SaR) operation fast localization of person(s) involved in the accident. Mountain SaR operations are common. For instance, during 2012 in France 5,389 operations have been registered by the French National Mountain Safety Observation System [1]. Two typical scenarios account for 62.2% of the mountain SaR interventions: the lost hiker and the avalanche. Hikers can be responsible for 59.41% of mountain SaR operations and 37% of these operations only consist of the searching of the person(s) [2]. When referring to snow sports (e.g. skiing, snowboarding), the most part of the accidents is caused by human-triggered avalanches and every year more than 150 people die because of avalanches in North America and Europe only [3],[4]. The fast localization of persons buried under the snow is crucial in these cases, as 60% of them die within the first 30 minutes [5]. The median of the burial depth avalanche victims is estimated to be as low as 1 m [6].

To support SaR operations for the person(s) involved in avalanche accidents two radiofrequency devices are currently used: the avalanche beacons (ARVA, regulated in the EU by the ETSI EN 300-718-1 [7]) and the RECCO® systems [8], comprising an interrogator that searches for reflectors. ARVAs transmit pulses in accordance with double sideband amplitude modulation with no modulating auxiliary carrier. The maximum pulse period is 1300 ms and a duty cycle between 5.4% and 69%. The transmission power is regulated so that the output field strength is comprised between -6 dBμA/m and 7 dBμA/m at a distance of 10 m and at the frequency of 457 kHz. The usage of Unmanned Aerial Vehicle (UAV) to localize the subjects is currently under study [9], [10], but ARVA-equipped drones have to deal with the poor performances of the current antennas, which are designed to be as small as possible and to be comfortable for the wearer [11]. The usage of UAV can be enabled by using technology with a longer radio range.

Still unexplored options for SaR applications concern the possible adoption of the emerging Low-Power Wide-Area Network (LPWAN) technologies including LoRa, Sigfox and NB-IoT. The LPWAN technologies are characterized by a significant long communication radio range and a low battery power consumption as compared to the standard wireless local area network technologies [12]. This is achieved at the expense of low data rate because of regulatory limitations imposing a low duty cycle for these systems, [13]. One of the most promising LPWAN technologies is LoRa (Long-Range) which was proven to reach up to 30 km of range [14]. LoRa system has a proprietary

The research leading to these results has received funding from the European Regional Development Fund under the Cooperation Programme Interreg V-A Italia Austria 2014-2020, ITAT3023, Smart Test for Alpine Rescue Technology START and from the European Regional Development Fund, Operational Program Investment for growth and jobs ERDF 2014-2020 under Project number ERDF1094, Data Platform and Sensing Technology for Environmental Sensing LAB-DPS4ESLAB.

Giulio Maria Bianco is with the Pervasive Electromagnetics Lab, University of Rome Tor Vergata, Rome, Italy, and also with the Center for Sensing Solution, EURAC research, Bolzano, Italy. Email: *giuliomaria.bianco@uniroma2.it* (contact author)

Gaetano Marrocco is with the Pervasive Electromagnetics Lab, University of Rome Tor Vergata, Rome, Italy.

Romeo Giuliano is with the Department of Innovation & Information Engineering, Guglielmo Marconi University, Rome, Italy.

Franco Mazzenga is with the Department of Enterprise Engineering "Mario Lucertini", University of Rome Tor Vergata, Rome, Italy.

Abraham Mejia-Aguilar is with the Center for Sensing Solutions, EURAC Research, Bolzano, Italy.

Physical Layer (PHY) and adopts Chirp Spread Spectrum (CSS) [15] modulation technique. It is often used with a Medium Access Control (MAC) called LoRaWAN issued by the LoRa Alliance [16]. LoRa PHY can even be used bypassing the MAC protocol layer. In this case, the LoRa radio is working in *"LoRa-MAC"* (or *"raw LoRa"*) mode [17] and broadcasts its messages on the selectable channel. Several LPWAN performance assessments have been published during recent years: in [18] the main LPWAN are compared with different technologies as the Bluetooth Low Energy and Near Field Communication; in [19] LoRaWAN performances and its QoS (Quality of Service) are tested; in [20] LoRaWAN networks are studied in dense urban and forest scenario. Regarding localization, LoRa has been mainly used to transmit position data from the associated GPS device [21]. Moreover, the LoRa signal-based localization has been presented and analyzed in the literature using different approaches [22]-[26]. In [22], [23] authors consider Received Signal Strength Indicator (RSSI) localization in cellular mobile radio assuming the Path Loss (PL) of the area is known a priori or has been measured in advance. The PL model is used to map the measured PL into the transmitter-receiver distance to apply well-known formulae for achieving the position estimate. This method has an accuracy of about 20 m when the PL model is exactly identified and the shadowing effects are negligible. Authors in [22] improve the algorithm in [24] by proposing to select the best base station to be considered for the measurements. Although the accuracy improves, the considered RSSI-based method greatly suffers from the environment variability accounted for by the shadowing which introduces errors in PL and then in the measure of distances. As shown in the following, this is not the approach considered in this paper where the estimation of PL parameters is embedded into the algorithm operations and the effects of shadowing are smoothed over several PL measurements. This allows achieving a more accurate estimate of the transmitter's position.

Other methods applied to LoRa in [25] are based on the Time Difference of Arrivals (TDoA). In this case, the LoRa transmitter adds a timestamp to the emitted packet. The LoRa gateways, geo-localized by GPS, can evaluate the TDoA of the arrival packet so to estimate the position of the transmitter. This method does not rely on the knowledge of the PL model but has a localization error in the order of 300 m depending on the time resolution in the timestamp. The method in [26] adopts the fingerprinting to localize a receiver moving in a service area. This approach requires a preliminary phase for the characterization of the area where the receiver is moving. Several sample points are considered and for each one of them data for fingerprint are measured and stored in a database. To localize the receiver the measured fingerprint data are compared with those stored in the database to assess its position. Although this method provides more accurate estimates, it has several drawbacks mainly related to the (periodical) training phase that can be time-consuming and costly, especially for large service areas. Furthermore, the collected values represent a specific situation for radio propagation. This means that the presence of new obstacles (e.g. persons or vehicles) in the area can invalidate data stored in the database thus leading to inaccurate position estimate. Fingerprint method cannot be applied in mountain scenarios where the propagation scenario is significantly altered because of snowing, an avalanche or rockfalls.

In this paper, we investigate the possibility of using LoRa for SaR operations in snowy mountain scenarios as an alternative radio technology to the already existing standards such as ARVA and RECCO®.

To this purpose, we describe the principle architecture of a radio system for SaR operations based on LoRa technology for the localization of person(s) involved in the accident. We assume the person(s) is/are equipped with a body area network consisting of different types of sensors, one (or more) LoRa transmitting device(s) and intelligence governing the body network so to continuously monitor the health status of the person and to (automatically) enable the communications for the alerting and interacting with rescuers in the case of personal illness or accident.

To support the localization of persons involved in the accident we also consider a localization procedure based on LoRa-based PL measurements (automatically) reported by rescuers moving in the accident area to a Control and Command operation Centre (CCC). The position estimation procedure is derived by the work in [27] and it is extended to include weighting the PL measurements taken by the rescuers moving in the accident area. Due to the reduced extension of the accident area with respect to the urban scenarios in [27], we analyze the possibility of solving the position estimation problem of the person involved in the accident by using an exhaustive search restricted to the unknown position of the transmitter of the person to be rescued. In the simpler case, we assume the unknown position of the person is allowed to vary over a regular grid superimposed over the accident area. Furthermore, we assume calculations are carried out in the CCC on the basis of the PL measurements received from rescuers. It is observed that this approach avoids the usage of the optimum search algorithms in [27] that in many cases considered in this paper could not converge to the optimal solution i.e. the true position of the person to be rescued.

To assess the effectiveness of the proposed system and localization procedure in a realistic scenario, in the paper we provide LoRa PL models based on data collected during an experimental campaign in mountain environments. Three important scenarios have been considered: hiker moving inside a canyon, the LoRa transmitter lying on the snow, (e.g. unconscious person lying on the snow) and finally, the LoRa transmitter under the snow (e.g. the typical avalanche scenario). Since the LoRa receiver is body-worn, the proposed models account for the impact of the body on the LoRa radio propagation in such scenarios. Experimental PL models are then used to evaluate the accuracy performance of the proposed localization algorithm in the

considered scenarios through simulations. It is observed that the accuracy in position estimation can be on the order of few meters around the true position if the number of PL measurements provided by the rescuers to the CCC is large enough so to counteract the effects of the strong shadowing on PL observed from measurements.
Furthermore, from the analysis of experimental results, we have observed that the communication range of LoRa in the considered mountain scenarios is about five times larger than the range achievable with commercial ARVA devices. This result has strongly motivated our investigation on the possibility of using LoRa in mountain SaR operations. To the best of the authors' knowledge, this is the first work investigating even on the basis of experimental results, the possibility of adopting LoRa LPWAN technology for mountain SaR.
The paper is organized as follows. In Section II the PL measurement setup and testbeds are detailed. In Section III the considered model for the PL characterization is presented. The corresponding PL parameters are obtained from experimental measurements in Section IV for the considered scenarios. In Section V the algorithm for position estimation based on measured LoRa PL is introduced. The performance of the localization algorithm is analyzed in Section VI in terms of the achievable accuracy in the considered measured propagation conditions. In Section VII the architecture of the proposed LoRa system for SaR is presented and its components are detailed in Section VIII. In Section IX the SaR procedure based on the considered LoRa-based SaR system is detailed and the effectiveness of the system is estimated in terms of latency and power consumption. Finally, in Section X conclusions are drawn.

II. Experimental setup for Path Loss evaluation

To model the LoRa propagation in mountain environments, a measurement campaign has been conducted in December 2019. The hardware used and the testbed organization are presented and discussed in this Section.

A. Considered Hardware

The considered LoRa hardware consists of two LoPy-4 expansion boards in Figure 1.a [28]. Since the LoRa performances can greatly vary depending on the selected transmission parameters, based on [29] we selected the following set of parameters:

1) Transmission Power: the maximum allowed P_{Tx} in the EU $865 - 868$ MHz band compliant with the highest duty cycle (1%) admitted for LoRa device has been selected i.e. $P_{TX} = 14$ dBm.
2) Carrier Frequency (CF): the 868 MHz frequency is considered for the following reasons. Even though PL in the 433 MHz band is lower than in 868 MHz, the maximum transmitting power in that band is 10 dBm; furthermore, antenna dimensions at 433 MHz are bigger for a stated radiation efficiency; finally, since the 433 MHz band is narrower than the corresponding band at 868 MHz, a lower number of communication channels can be created [30].
3) Spreading Factor (SF): has been set to 7. Although a higher SF results in a lower receiver sensitivity [31], and thus a higher link budget, each unitary increase in SF halves the transmission rate thus doubling the transmission time (so the required time of sleep), energy consumption and the communication channel usage.
4) Bandwidth (BW): the BW increase lowers the receiver sensitivity but the data rate is increased because of the Time on Air (ToA) reduction. The BW was set at $BW = 125$ kHz.
5) Coding Rate (CR): CR can be set to be either 4/5, 4/6, 4/7 or 4/8. In order to minimize the ToA, we selected $CR = 4/5$.

The two LoPy-4 expansion boards are equipped with two commercial external antennas: one 868 MHz folded dipole and one 2.4 GHz full-lambda dipole used to communicate the system with a computer via WiFi. The boards are powered using lithium polymer batteries (LiPo batteries, output voltage 3.7 V, capacity 1100 mAh). The dimensions of the LoRa radio are $295\ mm \times 60\ mm \times 20\ mm$ and its weight is 50 g. Thus, this device is suitable as payload for UAV to gather the PL measurements needed by the algorithm in Section V.
We used commercial ARVA devices to compare their performance (PIEPS POWDER BT [32] in Figure 1.b). They have a nominal radio range of 60 m, which is the typical range of ARVAs [7]. Geolocation during measurements was obtained by means of a GNSS station Leica GS10 [33].

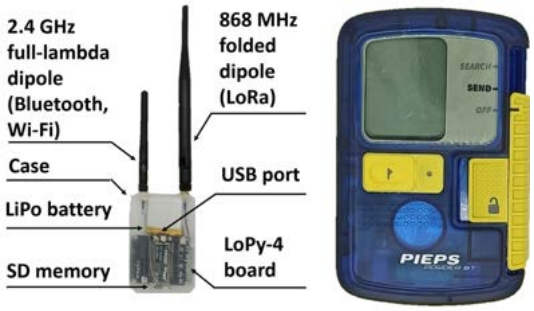

Figure 1. Devices used for the experiments: a) Lopy-4 expansion board tested; b) Reference ARVA: PIEPS POWDER BT.

B. Experimental Testbed

The PL data were collected by first considering two extremely harsh mountain environments: *i.* the bottom of a canyon for the lost hiker scenario and *ii.* a snowy field on the top of a mountain for the avalanche scenario. The scenario with the LoRa transmitter lying on the snow was also included in our experiments.
For the lost hiker scenario, the canyon in the Bletterbach park (Fig. 2.a) in northern Italy was selected as a testbed. The canyon maximum width, length and depth are about 40 m, 8 km and 400 m, respectively. The LoRa transmitter

(a) (b)

Figure 2. a) Bletterbach canyon; b) LoRa transmitting node placed on the ground.

(a) (b)

Figure 3. a) Lora receiver into a pocket of the volunteer's jacket; b) Body-worn ARVA.

was placed on the ground so to simulate an unconscious hiker in the middle of the canyon, around 5 m away from the water stream (Fig. 2.b). The LoRa device acting as a receiver was put inside the jacket of a volunteer (Fig. 3.a). This arrangement allowed resembling typical ARVA deployment (Fig. 3.b) and permitted to evaluate the effects of the body on the LoRa signal transmission. The transmitter sent packets, while the volunteer walked away from the transmitter over a radial direction. When the number of received packets dropped below 50% the volunteer stopped. PL measurements corresponding to a Packet Delivery Ratio (PDR) greater than 50% are assumed to be sufficiently accurate and fast to collect. To compare ARVA and LoRa, a transmitting ARVA device was placed in the same location as the LoRa transmitter. Then, the volunteer with ARVA walked following the same path of LoRa measurements so to estimate the maximum achievable ARVA radio range under the same propagation conditions. For the avalanche scenario, the selected test field was Campo Imperatore, on the top of Gran Sasso mountain (Italy; see Fig. 4.a). The field was covered by wet snow, which is known to hinder the communication range more than the dry snow [34]. The LoRa transmitting device was placed inside a watertight bag to protect the board from humidity. In this environment, two types of measurements have been executed: *i.* transmitter lying on the snow, with moving receiver and *ii.* transmitter buried under 1 m of snow (Fig. 4.b) and moving LoRa receiver. The same types of measurements were performed with

(a) (b)

Figure 4. a) Campo Imperatore field on the top of Gran Sasso mountain; b) The 1 m deep hole in the now used for burying the transmitter inside the watertight bag.

the ARVA devices. Data collected in the two different situations were used for the subsequent derivation of the parameters of the selected PL propagation models detailed in section IV.

III. Path Loss estimation from measurements and modeling

The PL has been evaluated on the basis of the measured RSSI and SNR (Signal-to-Noise Ratio) using the following equation:

$$PL = P_{Tx} + G_{Tx} + G_{Rx} + 10 \cdot Log_{10}\left(1 + \frac{1}{SNR}\right) - RSSI \quad (1)$$

where P_{Tx} is the transmission power, G_{Tx} and G_{Rx} are the gains of the transmitting and receiving antenna, respectively. The SNR is measured and returned by the chip in dB scale and then inserted in eq. (1) after dB-to-linear conversion.

The experimental PL data can be conveniently modeled using the first-order fit as done in [35], so that the considered Estimated Path Loss (EPL) model is:

$$EPL = PL_0 + 10 \cdot \gamma \cdot log_{10}(d/d_0) \quad (2)$$

where PL_0 is the PL intercept at the reference distance $d_0 = 1$ m and γ is the PL exponent. We assume the difference between the measured PL and EPL is due to shadow fading, whose standard deviation is:

$$\sigma_{SF} = std(PL - EPL) \quad (3)$$

where the EPL is the estimated PL model in (2).

In the literature, the PL of LoRa signals in different environments has been characterized by several measurement campaigns in different operating scenarios. The PL parameters for the lognormal PL model corresponding to the different scenarios are reported in Tab. I where the reference distance was set at 1 m for comparison purposes. To the best of the authors' knowledge, no existing LoRa PL model has been derived in a realistic setting where the LoRa device is worn in a jacket to account for (unavoidable) body effects. Furthermore, no PL models for LoRa in canyons or snowy mountain environments have been derived as well as LoRa PL models considering the LoRa transmitter buried under the snow (typical SaR scenario in the case of avalanche).

Table I
LOGNORMAL PL MODELS USED FOR LORA IN THE LITERATURE. THE σ_{SF} VALUE IS NOT AVAILABLE FOR ALL THE MODELS.

Frequency [MHz]	Environment	$PL(1\ m)[dB]$	Exponent	σ_{SF} [dB]
[14] 868	Sea	59.35	2.32	7.8
[14] 868	Urban	73.63	1.76	8.0
[30] 868	Urban	57.25	2.65	-
[30] 433	Urban	47	2.65	-
[36] 868	Urban	49.6	2.8	-
[37] 602	Suburban	36.35	2.49	-
[38] 900	Mountain (rocky field, no height)	55.75	2.82	8.9
[38] 900	Mountain (rocky field, 0.5 m height)	27.30	3.94	11.9

IV. PATH LOSS MODELS IN THE CONSIDERED SCENARIOS

A. Canyon: lost hiker scenario

A range of 51 m was observed for the ARVA devices (Fig. 5) inside the canyon. This result is in line with the nominal 60 m range declared by the manufacturers. Instead, the 50% PDR range measured for LoRa was 300 m (point-to-point GNSS observation) i.e. about six times the ARVA maximum range. The measured range is lower than the typical values of LoRa systems because the body-worn receiver is working in an extremely harsh environment characterized by body shadowing and reflections, and also by the impedance mismatch of the antenna.
The measured average PL for a 53% PDR was of 135 dB (see Tab. II) with a relatively small standard deviation. In [36] the estimated RSSI is about of -140 dBm when using $SF = 12$, corresponding to PL≅155 dB obtained using (1). This PL value is compatible with the measured values. In particular, it should be observed that moving from $SF = 7$ to $SF = 12$ leads to 13 dB variations in the receiver sensitivity [31]. From the measurements

Figure 5. Range measurements in Bletterbach canyon.

of RSSI and SNR, it was observed that a lognormal PL model for the canyon scenario provides good fitting. Because of the canyon topology, the channel propagation changes when passing from Line-of-Sight (LoS) to Non-Line-of-Sight (NLoS) at a distance of 163 m. However, this sudden change is not so evident in the PL. This is

Table II
MEASURED STATISTICS AT A DISTANCE OF 300 M FROM THE TRANSMITTER IN THE CANYON.

Distance (radial)	300 m
Average PL	135.4 dB
PL std	0.9 dB
PDR	53%
Number of packets sent	150

Table III
CANYON PATH LOSS PARAMETERS.

Environment	Canyon	Free Space
EPL exponent (γ)	5.51	2
EPL intercept ($PL\,(d_0)$) $[dB]$	0.9	31.2
σ_{SF} [dB]	10.13	
Number of packets sent	206	

possibly due to a sort of waveguiding effect in the canyon at the considered transmission frequencies. Collected data with the superimposed PL measurements are shown in Fig. 6. Model parameters are reported in Tab. III and they are compared to the Free Space (FS) model. The

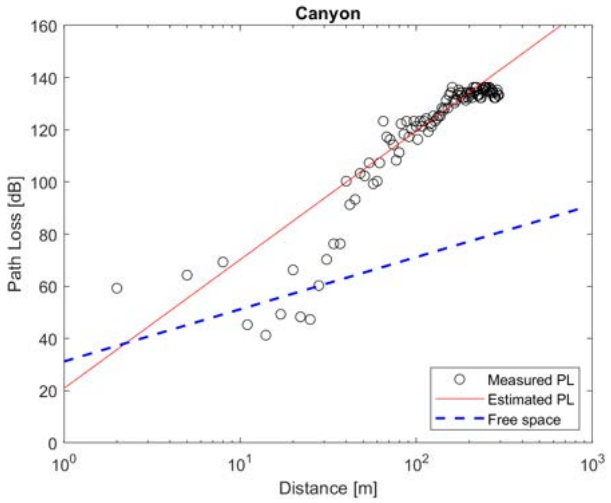

Figure 6. LoRa (868 MHz) estimated and measured PL in canyon compared with the free space model.

standard deviation σ_{SF} of shadowing is high due to the harsh environment. The relatively large value of the PL exponent, which is of the same order of that observed for NLoS propagation in buildings [39], accounts for the presence of obstacles influencing propagation. The model fitting of data in Fig. 6 appears to be valid at distances greater than about 20 m, whereas at closer distances the PL measurements appear to be unstable. This is mainly due to the prevalence of body shadowing effects, that affect propagation at smaller distances and can greatly vary depending on the position of the body with respect to the transmitter.

B. Top of the mountain: above/under the snow scenarios

The range measured with the ARVA with the transmitter over the snow was 64 m, greater than the nominal

range. The measured 50% PDR LoRa range under the same conditions is about 332 m, which is similar to the range measured in the canyon. In this case, it seems the main problems to propagation are due to snow reflections and body shadowing. When the transmitter was buried 1 m under the wet snow, the operating ranges of LoRa and ARVA were more than halved. This fact is shown by the results in Fig. 7 and in Tab. IV. It is worth noticing that the 50% PDR range of LoRa is about five times the maximum radio range of ARVA. The range reduction is mainly due to the power losses introduced by the water content of the snow. The average PLs measured

Figure 7. Range measurements in Campo Imperatore.

Table IV
Maximum range measured in Campo Imperatore.

Technology	Max range [m]
LoRa (over snow), 50% PDR	332
LoRa (buried), 50% PDR	152
ARVA (over snow)	64
ARVA (buried)	27

Table V
Statistics at different radials distances when the transmitter is either lying on the snow or buried under 1 m of snow.

Transmitter position	Lying	Buried	Buried
Distance (radial)	332 m	152 m	0 m
Average PL	120.2 dB	134.9 dB	61.2 dB
PL std	9.5 dB	1,4 dB	10.8 dB
PDR	54%	46%	83%
Number of packets sent	150	150	300

at distances corresponding to a PDR of about 50% are reported in Tab. V and are consistent with that in Tab. II. The higher standard deviation of PL measured in the case of LoRa transmitter over the snow is due to snow reflections. From data collected in the case of the receiver just over the buried transmitter (Tab. V), the 1 m snow layer alone causes around 60 ± 10 dB of additional PL and decreases the PDR of almost 20%. Collected data with the fitted model corresponding to the case of the LoRa transmitter over the snow are shown in Fig. 8, whereas data for the buried transmitter with the corresponding fitted EPL model are reproduced in Fig. 9. In Tab. VI the PL parameters measured in the snowy field are reported. It is worth noticing that the data collected at close distances seem to have very different behavior in the two considered cases: when the transmitter is over the snow the data at close distances are more similar to the FS model, as observed from the canyon measurements (Fig. 6); when the transmitter is buried under the snow instead, the single-slope PL model fits well also at close distances, thanks to the PL introduced by the layer of snow. During the measurements three packets having PL $= 128 \pm 0.6$ dB were measured at close distances when the transmitter was placed on the snow, probably due to a malfunctioning of the receiver; those data were not included in the EPL but they are nonetheless reported in Fig. 8 and labeled as outliers. The values of σ_{SF} measured in the snowy field

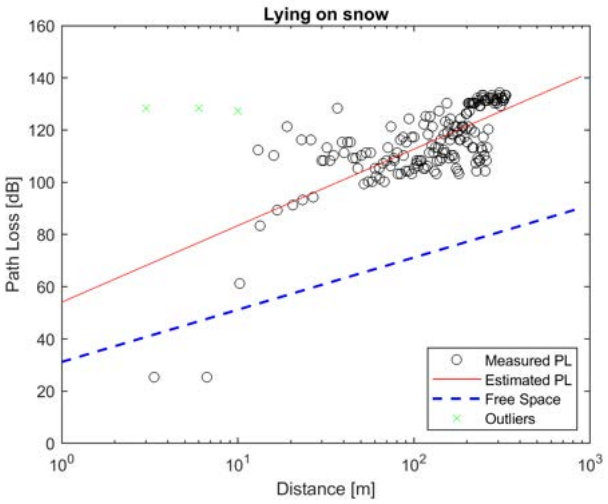

Figure 8. LoRa (868 MHz) estimated and measured PL when the transmitter is lying on the snow compared with the free space model.

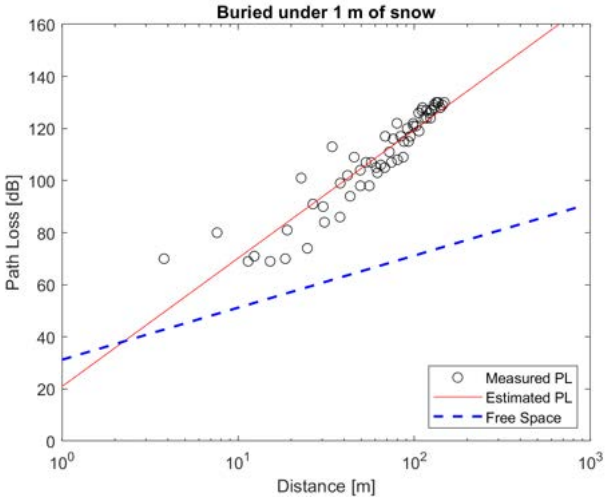

Figure 9. LoRa (868 MHz) estimated and measured PL when the transmitter is buried under 1 m of snow compared with the free space model.

Table VI
PL statistics measured in the snowy field.

Transmitter position	Lying	Buried	Free space
EPL exponent (γ)	3,17	4.93	2
EPL intercept ($PL(d_0)$)	56.7 dB	18.0 dB	31.2
σ_{SF}	9.95 dB	7.33 dB	
Number of packets sent	198	133	

(Tab. VI) are smaller than those measured in the canyon (Tab. III).

V. Localization algorithm for estimation of the transmitter position

In this Section, we detail the localization algorithm of the transmitter of the person involved in the accident. Taking into account for the EPL models derived in Section IV the transmitter can be localized using the algorithms in [27]. In this paper, we extend it by including the weighting of the Pl measurements and by considering a different approach for the calculation of the optimal solution.

While rescuers move in the incident area they record their GNSS positions. The received RSSI/SNR values by the rescuer are used to evaluate the corresponding PL. Let be PL_n, for $n = 1, \ldots, N$, the N measurements collected by the rescuers. They can be used to estimate the LoRa transmitter position associated with the injured person using the localization algorithm detailed in the following of this Section.

From [40] the unknown position (x_V, y_V) of the transmitter can be estimated based on the received PLs from the minimization of the following non-linear weighted mean square function:

$$\varepsilon(L_0, \gamma, x_V, y_V) = \sum_{n=1}^{N} w_n \left| PL_n - L_0 - 10\gamma \log_{10}(d_{n,V}^{(i)}) \right|^2 \quad (4)$$

The minimization is carried out with respect to the PL intercept constant $L_0 = PL(d_0)$ in (2), the PL exponent γ and to the unknown transmitter position (x_V, y_V). The distance $d_{n,V}^{(i)}$ in (4) is:

$$d_{n,V}^{(i)} = \sqrt{(x_n^{(i)} - x_V)^2 + (y_n^{(i)} - y_V)^2} \quad (5)$$

where $(x_n^{(i)}, y_n^{(i)})$ are the GNSS coordinates of the i-th rescuer providing the RSSI and the SNR data to the CCC to evaluate the n-th value of the PL for $n = 1, \ldots, N$, i.e. PL_n in (4). Minimization of (4) is usually achieved assuming homogeneous propagation scenario[1]. The minimization of (4) is a non-linear optimization problem with respect to the transmitter coordinates (x_V, y_V), only. In [27] the minimization of (4) is based on a non-linear gradient descent procedure. We observed that when this method is applied to our specific scenarios, many times it converges to a wrong solution even outside the search area.

In this paper, we propose a simple minimization algorithm based on the direct calculation of the two unknown variables L_0 and γ for a given (x_V, y_V). Then, we vary the values of (x_V, y_V) over a spatial grid superimposed over the search area. Taking into account that typical human-triggered avalanches areas do not extend for more than 100 $m \times 100$ m [3], we assume the coordinates (x_V, y_V) are allowed to vary over a regular square with a grid of points uniformly spaced along the x and y axes. For a given pair (x_V, y_V) the L_0 and γ minimizing (4) can be calculated in closed form by solving the following linear system of two equations:

$$\frac{\partial \varepsilon}{\partial L_0} = -2 \sum_{n=1}^{N} w_n \left(PL_n - L_0 - 10\gamma \log_{10}(d_{n,V}^{(i)}) \right) = 0 \quad (6)$$

and

$$\frac{\partial \varepsilon}{\partial \gamma} = -20 \sum_{n=1}^{N} w_n \left(PL_n - L_0 - 10\gamma \log_{10}(d_{n,V}^{(i)}) \right) \log_{10}(d_{n,V}^{(i)}) = 0 \quad (7)$$

Solutions $\hat{L}_0$ and $\hat{\gamma}$ of the system in (6) and (7) can be expressed in closed form as:

$$\hat{L}_0 = \frac{\sum_{n=1}^{N} w_n PL_n - 10\hat{\gamma} \sum_{n=1}^{N} w_n log_{10}(d_{n,V}^{(i)})}{\sum_{n=1}^{N} w_n} \quad (8)$$

and:

$$\hat{\gamma} = \frac{\sum_{m=1}^{N} w_m \sum_{n=1}^{N} w_n PL_n \log_{10}(d_{n,V}^{(i)}) - \sum_{m=1}^{N} w_m PL_m \sum_{n=1}^{N} w_n log_{10}(d_{n,V}^{(i)})}{10 \sum_{m=1}^{N} w_m \sum_{n=1}^{N} w_n \left(log_{10}(d_{n,V}^{(i)}) \right)^2 - 10 \left(\sum_{n=1}^{N} w_n \log_{10}(d_{n,V}^{(i)}) \right)^2} \quad (9)$$

Calculations in (8) and (9) are repeated for every point (x_V, y_V) in the considered grid. The point (x_V, y_V) corresponding to the minimum of (4) with respect to the other points in the grid is selected as the estimated transmitter position.

The weights w_n in (4) allows accounting for the quality of the PL measurements included in the position estimation algorithm. Since from experimental results it has been observed that in most cases inaccurate PL measurements can be obtained when the rescuer receiver is close to the transmitter location, these PLs should be "excluded" in some way by the optimization process. In particular, a low weight value w_n should be assigned to these measurements. This could be obtained in many ways. One simple approach could be to assign a low weight to those PL measurements below a threshold T_{PL}, e.g. $T_{PL} = 60$ dB looking for example at the experimental results in Figure 8. For simplicity, even $w_n = 0$ could be considered for these measurements. In principle, T_{PL} could be varied from a minimum to a maximum and the position estimation algorithm could be executed repeatedly for each value of T_{PL} discarding every time the corresponding PL measurements lying below the threshold. If the number of PL measurements is large enough there should be one value of T_{PL} (e.g. $\overline{T}_{PL}$) such that for $T_{PL} \geq \overline{T}_{PL}$ the fluctuations in the corresponding position estimates should become negligible.

The previous estimation algorithm can be further refined by considering a hierarchical exhaustive search approach. In particular, the exhaustive search over (x_V, y_V) can start over a regular grid over the emergency area with relatively large spaced test points. Grid points such that the error in (4) is below a given threshold are considered as the starting points for other exhaustive search using denser grids of points centred at the previously selected points.

[1]It should be noted that in the case of avalanche the propagation scenario tends to become homogeneous, at least from the point of view of rescuers. Thus, the assumption of considering homogeneous propagation environment in (4) can be considered reasonable in practice.

After this second stage only grid points providing error in (4) below a more stringent threshold are retained and used to start the third stage of exhaustive search and so on until the optimal point is determined. In the selection of the first grid, the spacing among points should be large enough to significantly reduce the number of position search trials but at the same time, they should be close enough to avoid the missing of the optimum position. This aspect can be crucial especially for those non-linear functions characterized by many local minimum points.

VI. Performance Results for the position estimation procedure

The accuracy of the location estimation algorithm in the presence of very strong shadowing affecting the PL measurements has been assessed by simulation. To this purpose, a synthetic propagation scenario was generated using the propagation models in Section IV with the corresponding parameters in Tables III-VI. A Monte-Carlo based approach is used to test the localization algorithm. In each trial, the transmitter position and the measurement points have been randomly generated in the area in accordance with a uniform spatial distribution. The number of PL measurements N has been varied between 5 and 300. For each scenario, a number of 10000 trials has been considered. To assess performance we have evaluated the mean and the standard deviation of the absolute value of the distance error between the true and estimated positions of the transmitter as a function of the number of available PL data N. The avalanche scenario with the buried transmitter has been considered first. In this case, the search area is a square of 100 m×100 m with a superimposed grid of search points at a distance of 1 m along the x and y axes. The PL models have been used to generate measurements of the PL each one affected by Normal distributed shadowing with standard deviation as in Tab.VI. We assumed a transmitting power $P_{Tx} = -10$ dBm, sufficient to cover the search area according to the models in Sec. IV. Since the lower PLs are supposed to be the nearest to the transmitter, we have weighted $w_n = 1/4$ the PLs lower than $T_{PL} = 50$ dB and with $w_n = 3/4$ the PLs higher than or equal to this threshold. Results have been reported in Fig. 10.

From the results, it can be observed that position estimation error rapidly decreases below a few meters for about 100 measurements. In a realistic operational scenario, it is important to achieve good position estimation accuracy in relatively small time i.e. this corresponds to process few measurements. This allows reducing the time required to achieve a first and sufficiently accurate estimate of the transmitter position so to rapidly coordinate rescuers to move towards the estimated position. The accuracy in the transmitter position estimation increases with the number of measurements allowing to average the impact of the strong shadow fading. Since the measured PLs are created from the EPL in Fig. 9 and they are spatially distributed in accordance with a uniform distribution, the percentage of measurements under the 50 dB PL threshold (i.e. within

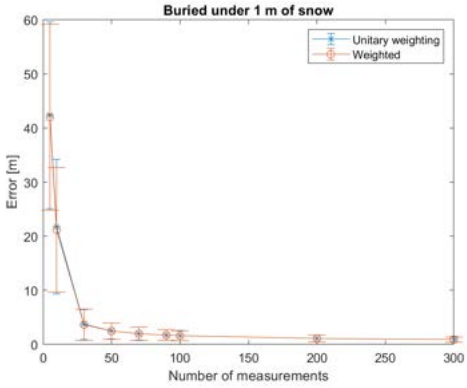

Figure 10. Localization error of the transmitter buried in snow over an area 100 $m \times 100$ m.

7 m of distance from the transmitter) is always about 2% of the overall number of measurements. Thus, as expected in this case the weighting has a negligible impact over the achievable localization error since the remaining 98% of measurements obscure the weighting effects. To assess

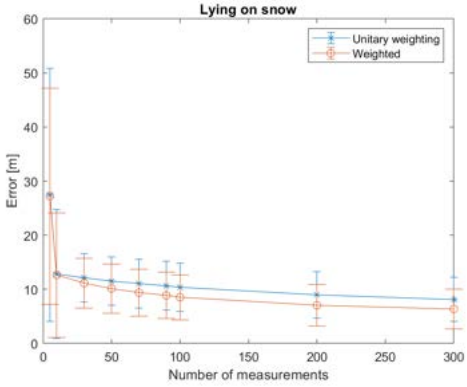

Figure 11. Localization error of transmitter placed on snow and 50% inaccurate measurements over an area 100 $m \times 100$ m.

the effectiveness of weighting, we considered the possibility of a non-uniform spatial distribution of measurements. In particular, we generated data from the EPL in Fig. 8 by including a large percentage of randomly generated PLs values at distances lower than 20 m from the transmitter. The generation range of these PL measurements has been set between 20 dB and 130 dB. It has been observed that when half of the received packets are received at distances lower than 20 m the localization error increases drastically (Fig. 11). In this case, weighting provides some benefit, by increasing the accuracy of more than 20% as shown in Fig. 12. Furthermore, from the simulations, it can be observed that the accuracy gain practically saturates when the number of measurements is $N \geq 200$.

Lastly, since the canyon can be modeled with an one-dimensional problem thanks to the waveguiding effect reported in Section IV-A, the accuracy of 3 m can be obtained with just $N = 30$ PL measurements, and accuracy of 1 m with $N = 50$ as shown in Fig. 13. It can be observed that the algorithm works fine despite the very

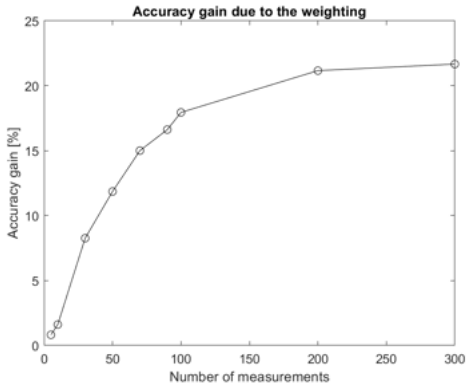

Figure 12. Accuracy improvement due to weighting in the case of Fig. 11 with respect to the non-weighting case.

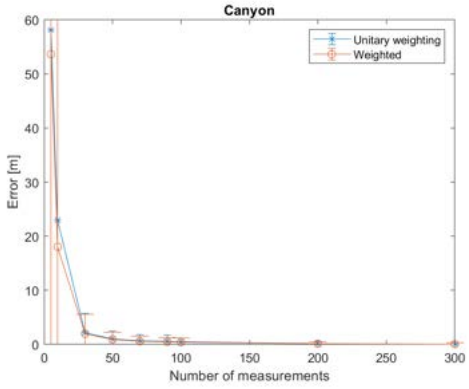

Figure 13. Localization error of transmitter in a canyon, search area of 1 $m \times 300$ m.

strong shadowing (standard deviation from 7 to 10 dB) measured in the three scenarios and that the adoption of weighting in the minimization allows improving the results in the worst-case of a high number of inaccurate measurements.

VII. Principle architecture of the system for SaR operations

In Figure 14.a we depict the principle scheme of the architecture of a LoRa-based system for supporting SaR operations. For illustration purposes, the avalanche event case has been considered. Due to the avalanche, one (or more) person(s) can be buried under the snow and they could be also unable to activate their signaling devices (i.e. ARVA or LoRa) to send an alert message. To avoid these problems, we assume the persons involved in the accident wear devices and sensors on their body so to realize a Body Area Network (BAN) governed by some intelligence. During normal conditions, the BAN intelligence continuously monitors through sensors measurements the health status of the person. In the case of an accident or any other dangerous event, data readings from local sensors can be used by the BAN intelligence to assess an abnormal situation affecting the person i.e. the BAN recognizes the imminent/persisting dangerous situation.

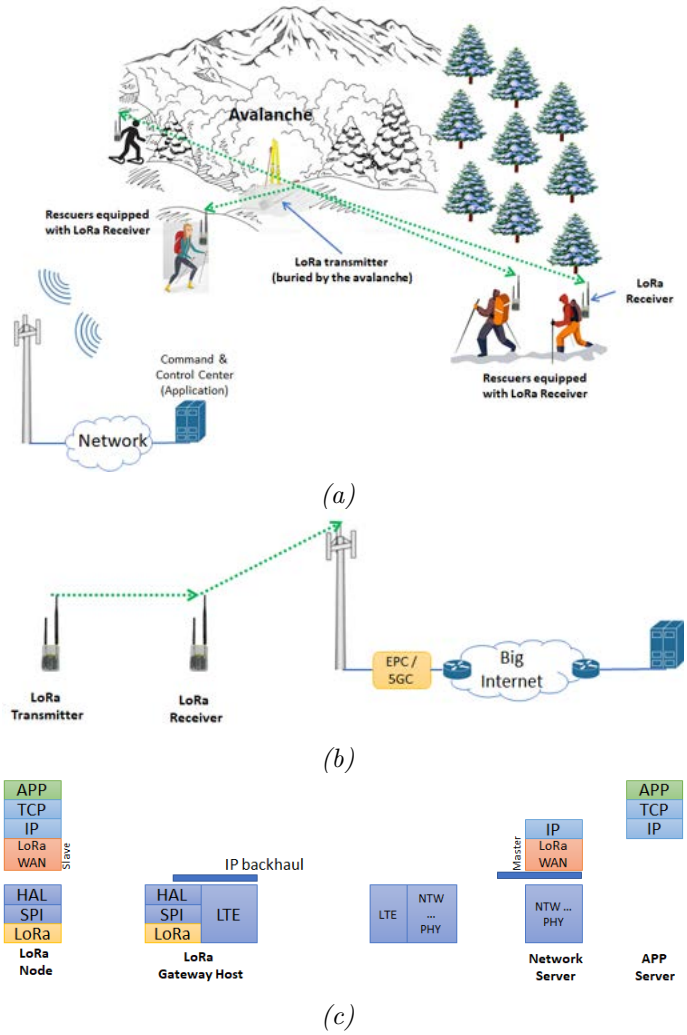

Figure 14. a) Sketch of the avalanche SaR scenario using LoRaWAN system; b) Principle scheme of the LoRa-based SaR system architecture; c) Possible LoRaWAN protocol stack for the proposed architecture.

This information can be used by the BAN intelligence to automatically send help request and (see after) to switch the LoRa transmitter device into the *Emergency Mode*. In Emergency Mode the LoRa transmitter starts to send Help Request Signals (HRSs) with a faster duty cycle than that recommended by regulatory authorities. This is necessary to efficiently support LoRa-based localization by rescuers of the person involved in the accident or in a critical situation. As shown in Figure 14 it is assumed that rescuers moving into the emergency area are equipped with LoRa receivers and are able to (automatically) perform PL measurements. These are forwarded to the CCC and given as input to the localization algorithm described in previous Section V. In particular, the CCC collects PL data to estimate the position(s) of the person(s), which in turn is (are) communicated by the CCC to the rescuers using all the available radio links (see Figure 14) covering the emergency area. As an example, they could use the (available) cellular radio technologies (e.g. 3G, 4G-LTE or the forthcoming 5G - see Figure 14.b), or they could use

the LoRa itself. In Figure 14.c we indicate one possible end-to-end (e.i. from the rescuer to/from the CCC) protocol stack architecture of the LoRaWAN system, which can be used to practically implement the communication system depicted in Figure 14.b. It is worth noticing that according to the deployed LoRaWAN model the LoRa transmitter, acting as a slave, creates a connection with its network server that can be reached using the IP backhaul link with the LoRa receiver acting as the LoRa gateway. The network server in the CCC acts as the master and runs the LoRa app to be used for the processing of the PL data sent by the rescuers.

VIII. Devices and localization in the considered LoRa SaR support system

In this Section, a discussion is provided concerning the design, the operational characteristics and additional functionalities of the devices to be integrated into the LoRa based rescue system in Fig. 14.

A. Device design for the user

The realization of a device for mountain SaR operations based on LoRa can exploit the great flexibility of LPWAN devices. The dimensions of the commercial ARVA model PIEPS POWDER BT are 118 $mm \times 76$ $mm \times 29$ mm and its weight is of 230 g. A LoRa-based transceiver with the same encumbrance can include:

1) *LoRa chip*: e.g. the SX1272 [41];
2) 868 *MHz near-isotropic antenna*: e.g. a turnstile antenna [42];
3) *BAN sensors*: to collect user's data and equipped with an on-board intelligence for making decisions about the health status and orientation of the person;
4) *Screen*: a screen which displays useful feedback to the user, regarding the transmitter status and its current working mode (Normal or Emergency Mode).

Focusing on the BAN, in the simpler case, we can assume it includes the following devices: one GNSS module, sensors for determining the orientation of the human body (i.e. ManDown sensors), sensors for measuring external pressure, temperature and haptic actuators. Even though the BAN is expected to be power consuming, wearable commercial devices integrating the proposed sensors are already available on the market [43]. We assume the BAN is equipped with one Emergency and one Reset Buttons. The pressing of the Emergency Button allows switching the BAN working mode from Normal to the Emergency after a few seconds. The Reset Button is necessary to return to normal mode or to stop sending HRS if the Emergency button has been inadvertently pushed by the BAN's owner, or the Emergency mode has been wrongly activated by the BAN intelligence. The haptic actuators are used to warn the user that the device is switching from Normal to the Emergency Mode.

B. Additional functionalities of the device for the SaR Rescuer

In our system, we assume the LoRa devices can be classified into two different classes: standard and rescue devices. Only the rescuers involved in the mountain SaR operations can be equipped with LoRa rescue devices. These include all the features of the standard LoRa devices and incorporate some important additional functionalities. During emergency operations, rescuers' LoRa transceivers commonly operate in receiving mode and could be equipped with a directional antenna (e.g. Yagi-Uda), which can be manually (or even automatically) oriented to reveal the direction of the maximum received signal power or RSSI. In addition, we assume the LoRa rescue transceiver should be able to broadcast an Emergency Activation Signal (EAS) to all the LoRa users' transceivers in the area. This can be obtained by means of a dedicated channel, which is used to send a 30-second long EAS. This signal can force the LoRa standard transceivers in the customers' BAN networks to commute from *Normal* into the *Emergency Mode*. A customer needing no help can use the Reset button to switch its transceiver into normal operation mode. This function is necessary to exclude from the rescuers' attention all customers needing no help. In fact, the extension of the LoRa area reached by the EAS can be larger than the emergency area. Thus some persons could be reached by the EAS even if they are not involved in the accident.

C. Detection and localization of persons involved in the accident

After EAS reception and/or after the BAN intelligence has assessed a distress condition of the person, the Emergency Mode is set and LoRa transceiver starts to send the HRS on a properly selected LoRa transmission channel. Rescuers devices continuously monitor for the presence of HRSs in the emergency area. Following the reception of the HRSs, the localization process can start on the basis of the PL measurements sent by the rescuers' moving into the emergency area to the CCC. The LoRa extended radio range allows rescuers to detect the HRS signals even when they are far from the position of the person involved in the accident. The principle of this operating procedure is similar to that based on ARVA. However, ARVA transceivers, characterized by short-range and hard degradation in the signal detection may render difficult the detection of the signal especially when the rescuers are far from the person involved in the accident. Hard degradation in ARVA signal detection is experienced when the received signal power is under the receiver sensitivity level. In this case, the ARVA receiver declares its impossibility to detect the presence of the signal. Instead, due to the possibility of changing the SF, LoRa can operate with different receiver sensitivities thus enabling HRS reception at distances larger than ARVA. In the Emergency Mode, even $SF = 12$ could be used to allow the LoRa receiver to operate at its lowest sensitivity. The possibility of a random selection of the

LoRa transmission channel is helpful to mitigate potential interference among LoRa transceivers belonging to more persons that could be involved in the accident. In principle, all the available LoRa channels in the $865-868$ MHz band could be used for supporting HRS transmission. Since up to 47 LoRa channels can be created in the EU 868 MHz unlicensed band using a BW of 125 kHz [44], to simplify the system design and protocol operations one channel can be assigned for the broadcast of the EAS while other channels can be dedicated to the HRSs.

D. LoRa Message Payload

A proposal for the payload of LoRa packets to be sent by the transmitter in the Emergency Mode is detailed below. The information fields of the considered payload are listed in the following points:

1) *Help Request*: one bit long, with 1 if the transmitter is working in Emergency Mode, 0 otherwise;
2) *Group ID* (optional): a number indicating the group identity of users the single user's transceiver belongs to. This field could be omitted if it is not necessary to identify the group of hikers/tourists visiting the mountain;
3) *Individual ID*: alphanumeric (randomly generated) string. This is the ID of the single LoRa transceiver and it is uniquely associated with its owner. Typically this ID is not displayed on the screen of the device in order to avoid ethical/privacy issues;
4) *GNSS availability status*: one bit, with 1 if the GNSS signal is available and 0 otherwise. A Rescue transceiver can ask for the transceiver to send the GNSS coordinates if they are available. In principle, the BAN could use the unavailability of GNSS signal as additional data to infer on possible dangerous/distress condition of the hiker.
5) *Temperature*: the value of sensed body temperature (in Celsius). This data is retrieved from the corresponding sensor integrated into the BAN;
6) *Pressure*: the value of external pressure (mbar). This data is measured from the sensor in the BAN network;
7) *ManDown*: one (or more) bit(s), in the simple case of one bit, the bit is set to 1 if the ManDown senses the user is fallen for more than 1 minute. In the case of more bits, the remaining bits could be used to indicate the status of gyroscopes in the BAN. These sensors could be used to determine if the person under the snow is in a non-natural position such as upside-down;
8) *WBAN* (optional): one bit, with 1 if the heart rate and the blood pressure sensed by additional BAN sensors (e.g. smartwatch) increases above some thresholds declared to be critical.

IX. SaR procedure and effectiveness of the proposed System

In this Section, we firstly provide a high-level description of the proposed SaR procedures for the person(s) involved in the accident and for the rescuer(s), and then we estimate the system's effectiveness in terms of end-to-end latency and power consumption.

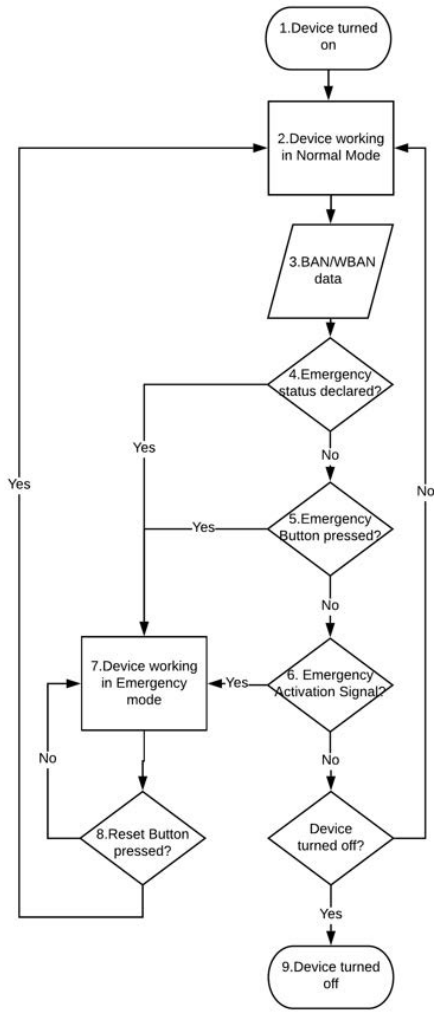

Figure 15. SaR procedure: user side.

A. Procedure: Person involved in the accident side

The diagram in Fig. 15 indicates the operations required by the user's BAN.

1) *BAN turned on*: it is assumed the person activates the BAN, while starts moving on the mountain. In most parts of Europe it is mandatory to worn and to turn on the ARVA device when skiing and for snowboarding. Similar regulatory rules could be enforced in the LoRa case.
2) *BAN in Normal Mode*: in Normal Mode, the LoRa device in the BAN sends packets 5 bytes long containing user's data in accordance with the duty cycle limitations i.e. the device emits 1 packet every 5 seconds. During the inactivity period, the LoRa device listens to the dedicated channel for the presence of an EAS from rescuers (see after); the reception of an EAS sets the status of the terminal to the Emergency Mode. Users not involved in the emergency can

restore the Normal status by pressing the Reset Button. As an alternative, the BAN intelligence can automatically restore the Normal Mode status in the case no anomaly is assessed.

3) *BAN data*: BAN devices continuously collect data from sensors; BAN intelligence analyzes them to assess for the presence of abnormal conditions. Additional information can optionally be collected from other devices such as the heart rate from a smartwatch. Smartwatches or any other external sensor can communicate with the BAN by means of a local wireless link based for example on Bluetooth Low Energy.
4) *Declaration of the Emergency status from the BAN without EAS reception*: data from local sensors allow BAN intelligence to assess the presence of anomalous situation and/or ongoing critical situation. If a critical situation is detected, the Emergency Mode status is automatically set by the BAN and a timer starts; if the BAN inadvertently activates the emergency status the user is required to press the Reset Button if he/she needn't help before the timer elapses. If the timer elapses, it is assumed by the BAN intelligence the user is unable to manually activate the Emergency Mode. In this case, the BAN intelligence turns the LoRa transceiver into the Emergency Mode and starts to send the HRS messages.
5) *Emergency Button*: even though an emergency could be not detected by the BAN, the user can always press the Emergency Button to require help.
6) *Emergency Activation Signal from rescuers*: in Normal Mode, when the LoRa transceiver is not transmitting it listens to the dedicated channel for any possible EAS sent by a Rescue transceiver. The reception of the EAS message turns the BAN and the LoRa transceiver into the Emergency Mode.
7) *BAN in Emergency Mode*: in Emergency Mode, the BAN and then the LoRa transceiver operates in a de-regulated mode i.e. by removing the LoRa duty cycle limitation of 1% so to reach a higher message rate e.g. 1 message every 2 seconds. In this case, the LoRa transmissions follow the protocol described in the previous Section i.e. random selection of the transmission channel and, for example, SF set to $SF = 12$ for the lowest sensitivity.
8) *Reset Button*: under any operating condition, the user can always press the reset button to reset the transceiver into Normal Mode.
9) *BAN turned off*: when the person is not involved in any mountain activity her/his BAN should be turned off so to let the LoRa transmission channels free.

It is useful to point out that the Emergency Mode can be raised by the user himself as well as set automatically by the BAN. This last feature allows launching alarms when the user is unconscious and/or buried in the snow and/or he/she is unable to manually switch the BAN to the Emergency Mode.

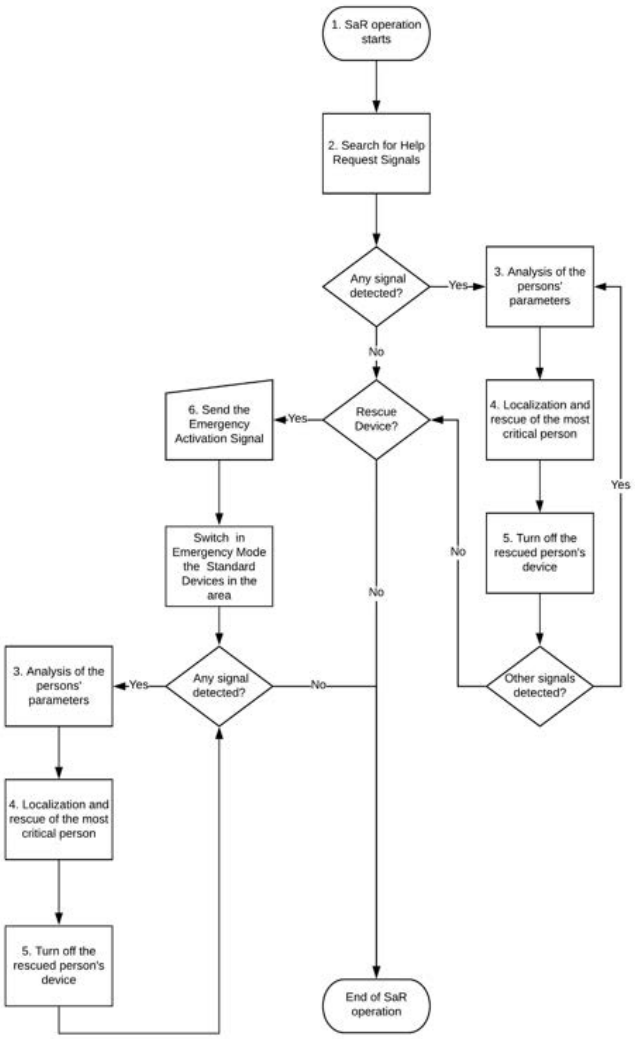

Figure 16. SaR procedure: rescuer side.

B. Procedure: Rescuer side

Rescuers follow the procedure indicated in Fig. 16. The procedure can vary in accordance with the category of rescuers' equipment, which may consist of a standard transceiver or the rescue transceiver (see Section VIII-B):

1) *Starting of SaR operation*: rescuers moving in the emergency area turn on their LoRa transceivers, which start working in the receiving mode.
2) *Searching for HRS*: the rescuers' transceivers search for the presence of HRSs by rapidly scanning the LoRa channels.
3) *Analysis of the persons' parameters*: the received HRSs contain information on the vital data allowing the rescuers to infer on the clinical status of the person involved in the accident.
4) *Localization of the most critical person*: for each received HRS the corresponding measurements of RSSI and SNR (or equivalently the locally calculated PL) are sent to the CCC to allow the estimation of the position of the person(s) involved in the emergency.

5) *Turn off the BAN LoRa device*: the transceivers of the rescued persons are turned off (eventually by remote action) so to decrease the LoRa channels usage.
6) *Emergency Activation Signal*: if the rescuer is equipped with a rescue transceiver he can emit EASs to automatically turn the standard devices into the Emergency Mode; this option is helpful to assess the presence of injured persons in the emergency area that are unable to manually activate the Emergency Mode and for some unpredictable reasons, the BAN intelligence was unable to set the Emergency Mode.

As outlined in the previous points, the measured RSSI and SNR including the GNSS coordinates of the rescuer are sent to the CCC for the processing required to estimate the position(s) of the person(s) using the localization algorithm discussed in Section V. The estimated position could then used by the director of the SaR to coordinate the movements of the rescuers in the area to converge to the estimated point.

C. Assessment of the end-to-end Latency

To assess the effectiveness of the proposed system it is of interest to evaluate the time taken to detect and localize the person since receiving the first emergency messages until localization by the CCC. We indicate this time as end-to-end latency. To this purpose, we need to evaluate the following three main contributions to end-to-end latency.

1) The time required for the CCC to collect N measurements from rescuers. This number should be selected to guarantee the desired estimation accuracy and it could be inferred for example by the curves depicted in Figure 10 (buried scenario). In general, in any scenario, it seems $N \geq 50$ can provide an initial acceptable estimation accuracy of the transmitter position that can be improved as the CCC receives new measurements. Indicating with R_m (msg/s) the message generation rate from the transmitter in the Emergency Mode and K the number of rescuers receiving the emergency messages, the time $T_m(N)$ required to collect N PL measurements is:

$$T_m(N) = \frac{N}{R_m K} \tag{10}$$

and $R_m K$ is the number of PL data collected by K rescuers in the unit of time.
2) The time T_{TX} required to the rescuers to send PL data at the CCC for each received HRS. We assume the transmission capacity of the radio mobile channel is large enough to allow the rescuers to send PL data to CCC almost simultaneously. From the scheme, in Figure 14 the T_{TX} is the sum of the contributions listed and detailed in Table VII. For this evaluation we have considered the maximum serialization delay in LoRa i.e. we assume data are sent to CCC by rescuers using the lowest available bit rate in LoRa $R_b = 300$ bit/s. Obviously to reduce latency higher bit rates can be considered. The delays for transmissions in the mobile radio network connecting the rescuers to the CCC have been taken from [45].

Table VII
THE TIME REQUIRED FOR THE RESCUERS TO SEND THE DATA TO THE CCC.

Contribution	**Time [ms]**
Tx-Rx LoRa link (for $R_b = 300$ bit/s)	133.3
LoRa GW-to-eNB (eUTRAN)	18.3
ACCESS-to-CORE (EPC)	10
CORE-to-SERVER (Big Internet)	5
Total	**166.6**

3) The time $T_{P,R_X}(N)$ required for processing the N measurements in the CCC to estimate the position of the transmitter and to return this information to the rescuers in the emergency area. From the definition $T_{P,R_X}(N)$ is:

$$T_{P,R_X}(N) = T_{srv}(N) + T_{CCC,TX}, \tag{11}$$

and $T_{srv}(N)$ is the time required to process N measurements in accordance with the algorithm in Section V. To evaluate this delay we refer to the profiling results obtained from the MATLAB implementation of the algorithm. The software runs over an Intel I7 octa-core processor with 16 GBytes of memory clocked at 3.6 GHz. We obtained the following results: $T_{srv}(N) = 686$ ms for $N = 50$, $T_{srv}(N) = 816$ ms for $N = 100$ and, finally, $T_{srv}(N) = 1020$ ms for $N = 200$. It should be noticed that when $N = 50$ measurements have been collected we obtain a first good estimate of the actual position of the transmitter. This estimate can be immediately sent to rescuers so that they can move towards the target. While the rescuers are moving they continue to transmit PL data to the CCC which uses the new measurements to further refine the position estimate. Finally, the $T_{CCC,TX}$ is the time required by the CCC to send information position to the rescuers. It can be calculated as the sum of the components indicated and detailed in Table VIII, [45].

Table VIII
THE TIME REQUIRED FOR THE CCC TO SEND THE DATA TO THE RESCUERS.

Contribution	**Time [ms]**
SERVER-to-CORE	5
CORE-to-wireless ACCESS (EPC)	10
BS-to-RESCUERS	6.5
APP Processing	4
Total	**25.5**

Summing the three delay components, the overall latency $T(N)$ to obtain a first estimate of the position of the transmitter is:

$$T(N) = T_m(N) + T_{TX} + T_{P,R_X}(N). \tag{12}$$

Some results for $T(N)$ have been reported in Table IX for different N, numbers of rescuers K and R_m. The dominant

Table IX
ESTIMATED LOCALIZATION LATENCY [S] FOR SOME VALUES OF N, K AND R_m.

	Number of Measurements, N					
Number of	50		100		200	
Rescuers, K	1msg/5s	1msg/2s	1msg/5s	1msg/2s	1msg/5s	1msg/2s
1	250,88	100,88	501,01	201,01	1001,21	401,21
5	50,88	20,88	101,01	41,01	201,21	81,21
10	25,88	10,88	51,01	21,01	101,21	41,21

contribution in (12) is the time required for collecting measurements, which can be reduced by increasing the number of rescuers and/or the rate of HRS per second, R_m.

D. Power consumption in the Emergency Mode

To assess the power consumption in the LoPy-4 boards used for measurements, we have measured a current of $I_{SB} = 105.38$ mA in standby condition[2]. When switching the device in transmission mode with 1 msg every 5 s we have measured an average current absorption of $I_5 = 140$ mA. Considering now an increased message rate to 1 msg every 2 s the absorption rises to $I_2 = 192$ mA. From these figures is immediate to evaluate power consumption of the device taking into account that the voltage by the power supply is 5 V. Finally, it is of interest to calculate the battery life when the terminal is in the Emergency Mode. Assuming the device is equipped with a LiPo battery of 1100 mAh, this allows remaining in the Emergency Mode for about 5 h and 45 min.

X. CONCLUSION AND FUTURE WORK

In this paper, we have demonstrated that LoRa can be effectively used in Search and Rescue operations. We have first characterized the LoRa Path Loss in three relevant mountain scenarios: canyon, LoRa transmitter over the snow and transmitter buried under the snow. The models account also for the effects of the human body. We showed that the radio range achievable with LoRa is about five times larger than the ARVA range in the same propagation conditions. This allows starting the localization of person(s) involved in the accident even when rescuers are far from his/her position. To this purpose, we have developed a localization algorithm that can be applied to estimate the position of injured persons. The algorithm is simple to implement and operates on the basis of the PL measurements collected by the rescuers while moving into the emergency area. To assess the effectiveness of the proposed algorithm in a realistic scenario, we tested the algorithm on the basis of the experimental measurements. It has been observed that the achievable localization accuracy can be in the order of a few meters from the true position of the injured person. The localization algorithm can be seen as a tool in the proposed LoRa-based system for supporting SaR operations. In the proposed system, we have assumed persons are equipped with a Body Area Network consisting of different types of sensors and including one LoRa transmitting device. The BAN is equipped with some intelligence able to make autonomous decisions on the basis of the monitored health status of the person. Detection by BAN of distress condition allows automatically setting the LoRa transceiver into the Emergency Mode so to promptly alert rescuers. A high-level description of the procedures governing the operations of the proposed rescue system has been provided in the paper.

Some of the authors are currently working with the Center for Sensing Solution of EURAC research on developing and testing the proposed system in the Bletterbach canyon (Bolzano, Italy) to experimentally assess the system's performances. In the proof of concept which is currently under test, a UAV is equipped with one LoRa receiver to collect the measurements and automatically localize the transmitter. After the prototype validation in a laboratory, we will conduct an experimental campaign with the Italian mountain rescue (CNSAS) in Bletterbach to compare the traditional protocols to find missing persons with the one proposed in this paper. Afterwards, we will replicate the solution to monitor simultaneously hundreds of visitors towards a geospatial platform specifically oriented to the Internet of Things.

[2]It should be remarked that this value refers to the current absorption of the entire device and not of LoRa. This is also in line with the figure reported in the data sheet of the LoPy-4 board [28].

REFERENCES

[1] B. Soule', B. Lefe'vre, E . Boutroy, V. Reynier, F. Roux, and J. Corneloup, "Accidentology of mountain sports", Situation, review & diagnosis, Crolles, 2014.

[2] R. Sadeghi , J. C. Konwinski, R. K. Cydulka, "Adirondack Park Incidents: A Retrospective Review of Search and Rescue Reports From 2008 and 2009", Wilderness & Environmental Medicine, Volume 26, Issue 2, 159 - 163.

[3] J. Schweizer and G. Krüsi, "Testing the performance of avalanche transceivers", Cold Regions Science and Technology, vol. 37, no. 3, pp. 429-438, 2003.

[4] K. Grasegger, G. Strapazzon, E. Procter, H. Brugger and I. Soteras, "Avalanche Survival After Rescue With the RECCO Rescue System: A Case Report", Wilderness & Environmental Medicine, vol. 27, no. 2, pp. 282-286, 2016.

[5] V. Ferrara, "Technical survey about available technologies for detecting buried people under rubble or avalanches", WIT Transactions on The Built Environment, vol. 150, pp.91-101, 2015.

[6] F. Tschirky, B. Brabec, M. Kern, "Avalanche Rescue Systems in Switzerland: Experience and Limitations", Proceedings of International Snow Science Workshop, Big Sky MT, USA, 1-6 October 2000, pp. 369–376.

[7] European Telecommunications Standards Institute, "ETSI EN 300 718-1 V2.1.0", 2017. Accessed on: 15 Jan, 2020. [Online]. Available: https://www.etsi.org/deliver/etsi_en/300700_300799/30071801/02.01.00_20/en_30071801v020100a.pdf

[8] M. Stanford, "Use of Recco System to Locate Buried Roads in a Winter Environment", Proceedings of the 1994 International Snow Science Workshop, Snowbird, Utah, USA, 1994

[9] S. Bories, K. Allabouche and N. Daniele, "Recent Development on Search of Avalanches Victims with Monopulse Antenna mounted on a small UAV," 2019 13th European Conference on Antennas and Propagation (EuCAP), Krakow, Poland, 2019, pp. 1-4.

[10] V. Wolfe, W. Frobe, V. Shrinivasan and T. Hsieh, “Detecting and locating cell phone signals from avalanche victims using unmanned aerial vehicles,” 2015 International Conference on Unmanned Aircraft Systems (ICUAS), Denver, CO, 2015, pp. 704-713.

[11] D. Macii, G. Filippetto and M. Donelli, “Measurement of equivalent circuit parameters of avalanche beacons antennas for rapid prototyping,” 2017 IEEE International Workshop on Measurement and Networking (M&N), Naples, 2017, pp. 1-6.

[12] K. Phung, H. Tran, Q. Nguyen, T. Huong, T. Nguyen, “Analysis and Assessment of LoRaWAN,” 2018 2nd International Conference on Recent Advances in Signal Processing, Telecommunications & Computing (SigTelCom), 2018.

[13] K. Mekki, E. Bajic, F. Chaxel and F. Meyer, “Overview of Cellular LPWAN Technologies for IoT Deployment: Sigfox, LoRaWAN, and NB-IoT,” 2018 IEEE International Conference on Pervasive Computing and Communications Workshops (PerCom Workshops), Athens, 2018, pp. 197-202.

[14] J. Petajajarvi, K. Mikhaylov, A. Roivainen, T. Hanninen and M. Pettissalo, “On the coverage of LPWANs: range evaluation and channel attenuation model for LoRa technology,” 2015 14th International Conference on ITS Telecommunications (ITST), Copenhagen, 2015, pp. 55-59.

[15] V. Talla, M. Hessar, B. Kellogg, A. Najafi, J. R. Smith and S. Gollakota, “LoRa backscatter: Enabling the vision of ubiquitous connectivity,” Proc. ACM Interact. Mobile Wearable Ubiquitous Technol., vol. 1, no. 3, Sep. 2017, Art. no. 105.

[16] LoRa Alliance, “LoRa specification”, LoRa Alliance, 2015. Accessed on: Jan. 15 2020. [Online]. Available: http://bit.ly/LoRaWAN-specification.

[17] Pycom company, “Pycom Ation Wi Py 3.0 User Guide”, Pycom company, 2017. Accessed on: Jan. 15, 2020. [Online]. Available: https://usermanual.wiki/Document/Pycom20WiPy203020user20guide.1505216624/htm

[18] C. Gomez, A. Minaburo, L. Toutain, D. Barthel and J. C. Zuniga, “IPv6 over LPWANs: connecting Low Power Wide Area Networks to the Internet (of Things)”, IEEE Wireless Communications Magazine, 2019

[19] E. D. Widianto, M. S. M. Pakpahan, A. A. Faizal and R. Septiana, “LoRa QoS Performance Analysis on Various Spreading Factor in Indonesia,” 2018 Int. Symposium on Electronics and Smart Devices (ISESD), Bandung, 2018, pp. 1-5

[20] M. R. Villarim, J. V. H. de Luna, D. de Farias Medeiros, R. I. S. Pereira and C. P. de Souza, “LoRa Performance Assessment in Dense Urban and Forest Areas for Environmental Monitoring,” 2019 4th Int. Symposium on Instrumentation Systems, Circuits and Transducers (INSCIT), Sao Paulo, Brazil, 2019, pp. 1-5.

[21] A. T. Nugraha, R. Wibowo, M. Suryanegara and N. Hayati, “An IoT-LoRa System for Tracking a Patient with a Mental Disorder: Correlation between Battery Capacity and Speed of Movement,” 2018 7th International Conference on Computer and Communication Engineering (ICCCE), Kuala Lumpur, 2018, pp. 198-201

[22] K. Lam, C. Cheung and W. Lee, “New RSSI-Based LoRa Localization Algorithms for Very Noisy Outdoor Environment,” 2018 IEEE 42nd Annual Computer Software and Applications Conference (COMPSAC), Tokyo, 2018, pp. 794-799

[23] P. Savazzi, E. Goldoni, A. Vizziello, L. Favalli and P. Gamba, “A Wiener-Based RSSI Localization Algorithm Exploiting Modulation Diversity in LoRa Networks,” in IEEE Sensors Journal, vol. 19, no. 24, pp. 12381-12388, 15 Dec. 15, 2019.

[24] K. Lam, C. Cheung and W. Lee, “LoRa-based localization systems for noisy outdoor environment,” 2017 IEEE 13th International Conference on Wireless and Mobile Computing, Networking and Communications (WiMob), Rome, 2017, pp. 278-284,

[25] S. Kim, J. Ko, “Low-complexity outdoor localization for long-range, low-power radios”, Proceedings of the 14th Annual International Conference on Mobile Systems, Applications, and Services Companion, Singapore, 26 June 2016; p. 44.

[26] W. Choi, Y.-S. Chang, Y. Jung, J. Song, “Low-Power LoRa Signal-Based Outdoor Positioning Using Fingerprint Algorithm;” ISPRS Int. J. Geo-Inf, 2018, 7, 440.

[27] X. Li, “RSS-Based Location Estimation with Unknown Pathloss Model,” in IEEE Transactions on Wireless Communications, vol. 5, no. 12, pp. 3626-3633, December 2006.

[28] Pycom Company, ”Pycom_002_Specsheets_LoPy4_v2”, Pycom Company, 2017. Accessed on: Jan. 15, 2020. [Online]. Available:https://docs.pycom.io/gitbook/assets/specsheets/Pycom_002_Specsheets_LoPy4_v2.pdf

[29] M. Bor and U. Roedig, “LoRa Transmission Parameter Selection,” 2017 13th International Conference on Distributed Computing in Sensor Systems (DCOSS), Ottawa, ON, 2017, pp. 27-34. doi: 10.1109/DCOSS.2017.10

[30] P. Jörke, S. Böcker, F. Liedmann and C. Wietfeld, “Urban channel models for smart city IoT-networks based on empirical measurements of LoRa-links at 433 and 868 MHz,” 2017 IEEE 28th Annual Int. Symposium on Personal, Indoor, and Mobile Radio Communications (PIMRC), Montreal, QC, 2017, pp. 1-6.

[31] [A. Augustin, J. Yi, T. Clausen and W. Townsley, “A Study of LoRa: Long Range & Low Power Networks for the Internet of Things,” Sensors, vol. 16, no. 9, 2016.

[32] Pieps GmbH, “Manual PIEPS PRO BT/POWDER BT | Firmware v1.1 | 08/2019”, Pieps GmbH, 2019. Accessed on: Jan. 1, 2020. [Online]. Available: https://www.pieps.com/sites/default/files/2019_08_08_propowderbt_manual_en-en.pdf

[33] Leica Geosystem Company, “Leica Viva GNSS Ricevitore GS10”, Leica Geosystem Company, 2012. Accessed on: Apr. 2, 2020. [Online]. Available: https://w3.leica-geosystems.com/downloads123/zz/gpsgis/Viva%20GNSS/brochures-datasheet/Leica_Viva_GNSS_GS10_receiver_DS_it.pdf

[34] RECCO company, “R9 detector user guide”, RECCO company, 2009. Accessed on: Jan. 15, 2020. [Online].Available: https://usermanual.wiki/RECCO/A-

[35] T. Ameloot, P. Van Torre and H. Rogier, “Indoor Body-to-Body LoRa Link Characterization,” 2019 IEEE-APS Topical Conference on Antennas and Propagation in Wireless Communications (APWC), Granada, Spain, 2019, pp. 042-047.

[36] M. R. Seye, B. Ngom, B. Gueye and M. Diallo, “A Study of LoRa Coverage: Range Evaluation and Channel Attenuation Model,” 2018 1st International Conference on Smart Cities and Communities (SCCIC), Ouagadougou, 2018, pp. 1-4.

[37] D. Plets *et alii*, “TDoA-Based Outdoor Positioning with Tracking Algorithm in a Public LoRa Network,” Wireless Communications and Mobile Computing, Wiley, doi: https://doi.org/10.1155/2018/1864209.

[38] T. O. Olasupo, "Wireless Communication Modeling for the Deployment of Tiny IoT Devices in Rocky and Mountainous Environments," in IEEE Sensors Letters, vol. 3, no. 7, pp. 1-4, July 2019, Art no. 6001204, doi: 10.1109/LSENS.2019.2918331.

[39] Tony J. Rouphael, “High-Level Requirements and Link Budget Analysis,” RF and Digital Signal Processing for Software-Defined Radio, 1st edition Burlington, Vermont, USA: Elsevier Newnes, 2009, ch. 4, sec. 2, p. 100.

[40] H. Nurminen et al., “Statistical path loss parameter estimation and positioning using RSS measurements in indoor wireless networks,” 2012 International Conference on Indoor Positioning and Indoor Navigation (IPIN), Sydney, NSW, 2012, pp. 1-9.

[41] Semtech Corporation, “SX1272/73 datasheet”, Semtech Corporation, California, USA, 2017. Accessed on: Merch 24, 2020. [Online]. Available: https://www.mouser.com/datasheet/2/761/sx1272-1277619.pdf

[42] S. X. Ta, I. Park and R. W. Ziolkowski, “Crossed Dipole Antennas: A review,” in IEEE Antennas and Propagation Magazine, vol. 57, no. 5, pp. 107-122, Oct. 2015.

[43] ProEsys s.r.l., “LoRaWAN/GNSS/Biosensor Wearable Tracker WearLOC-2”, ProEsys s.r.l., Italy, 2018. Accessed on: March 29, 2020. [Online]. Available: http://proesystech.com/wp-content/uploads/2018/02/Wearloc-2-datasheet.pdf

[44] K. Mikhaylov, J. Petaejaejaervi and T. Haenninen, “Analysis of Capacity and Scalability of the LoRa Low Power Wide Area Network Technology,” European Wireless 2016; 22th European Wireless Conference, Oulu, Finland, 2016, pp. 1-6.

[45] H. Holma, A. Toskala, T. Nakamura, “5G Technology: 3GPP New Radio”, First Edition, John Wiley & Sons Ltd., 2020